Earth and Planetary Science Letters 375 (2013) 395–407

Contents lists available at ScienceDirect

Earth and Planetary Science Letters

journal homepage: www.elsevier.com/locate/epsl

Seismic signatures of a hydrated mantle wedge from antigorite crystal-preferred orientation (CPO)

Sarah J. Brownlee [a,*,1], Bradley R. Hacker [a,b], George E. Harlow [c], Gareth Seward [a]

[a] Earth Research Institute, University of California, Santa Barbara, CA, USA
[b] Department of Earth Science, University of California, Santa Barbara, CA, USA
[c] Department of Earth and Planetary Sciences, American Museum of Natural History, New York, NY, USA

ARTICLE INFO

Article history:
Received 22 August 2012
Received in revised form
26 April 2013
Accepted 3 June 2013
Editor: L. Stixrude
Available online 28 June 2013

Keywords:
antigorite
seismic anisotropy
subduction
electron backscatter diffraction (EBSD)
CPO
LPO

ABSTRACT

We report electron backscatter diffraction (EBSD) measurements of antigorite crystal preferred orientations (CPOs) from 7 samples of antigorite schist from serpentinite mélanges adjacent to the Motagua fault system in central Guatemala. The CPOs range from diffuse girdle to point distributions of $(001)_{atg}$. Girdle distributions of $(001)_{atg}$ are not expected from deformation theory or experiments, suggesting that they are a result of growth rather than deformation, and may thus be topotactically related to the CPO of the olivine from which the antigorite grew. The calculated seismic anisotropy ranges from 6% to 28% in V_P, and 5% to 33% in V_S, and is highest for samples with a point maximum of $(001)_{atg}$. For all samples the minimum V_P corresponds to the pole to $(001)_{atg}$, and the maximum V_P occurs within the foliation for samples with a clearly defined foliation. Trench-parallel shear-wave splitting observations for subduction zones can best be explained by a combination of olivine B-type CPO and antigorite oriented with (001) parallel to the foliation; only a relatively thin (~20 km) zone of hydrated mantle is required to explain the observed splitting times.

1. Introduction

Hydration/dehydration reactions in the mantle wedge and slab of subduction zones have important effects on seismicity and seismic velocity, including velocity anisotropy (e.g., Hacker et al., 2003; Kneller et al., 2007; Rabbel et al., 2011). For instance, antigorite schist along the base of the mantle wedge has been proposed to explain trench-parallel fast shear-wave polarization planes observed in subduction zones (e.g. Katayama et al., 2009). Olivine B-type CPO, which can form in water-saturated conditions (Jung and Karato, 2001), has been suggested to contribute to trench-parallel shear-wave splitting in the fore-arc portion of mantle wedge (Kneller et al., 2007). Dehydration reactions in the subducting slab have been proposed to explain the double seismic zone observed in many subduction zones (Hacker et al., 2003; Brudzinski et al., 2007). The distribution of hydrous minerals within a subduction zone can be studied directly using seismic imaging if the seismic properties of hydrous minerals are significantly different from those of anhydrous minerals. This study investigates the effects of hydration in the mantle wedge of subduction zones by measuring the crystal-preferred orientation (CPO) of antigorite schists from the mélange adjacent to the Motagua fault system in central Guatemala.

2. Methods

2.1. Samples

Antigorite schist was collected from serpentinite mélanges adjacent to the Motagua fault system in central Guatemala (Fig. 1) as part of a study of the Guatemala Suture Zone (e.g., Harlow et al., 2006, 2011; http://research.amnh.org/eps/jade). Small chips ($\sim 3 \times 3 \times 1$ cm^3) were cut from samples that have "relatively coarse" antigorite prisms in thin section (Table 1), selected by GEH from the American Museum of Natural History (AMNH) collection. All but one sample (MVE03-60) come from the mélange north of the fault (Brueckner et al., 2009; Flores et al., 2010), however, except for subtle differences in assemblage statistics (Harlow et al., 2006, 2010), these antigorite schists from both sides of the fault are very similar. The samples are almost 100% antigorite with only a few vol% carbonates, oxides, and sulfides, talc and chlorite (Table 1); phases were identified with a combination of powder X-ray diffraction and microprobe analysis supported by optical petrography, plus the EBSD and EDS observations made in this study. Standard (30 μm thick) thin

* Corresponding author. Tel.: +1 313 577 6223.
E-mail addresses: sarah.brownlee@wayne.edu, brownlee.sj@gmail.com (S.J. Brownlee).
[1] Now at: Department of Geology, Wayne State University, Detroit, MI, USA.

0012-821X/$ - see front matter © 2013 Elsevier B.V. All rights reserved.
http://dx.doi.org/10.1016/j.epsl.2013.06.003

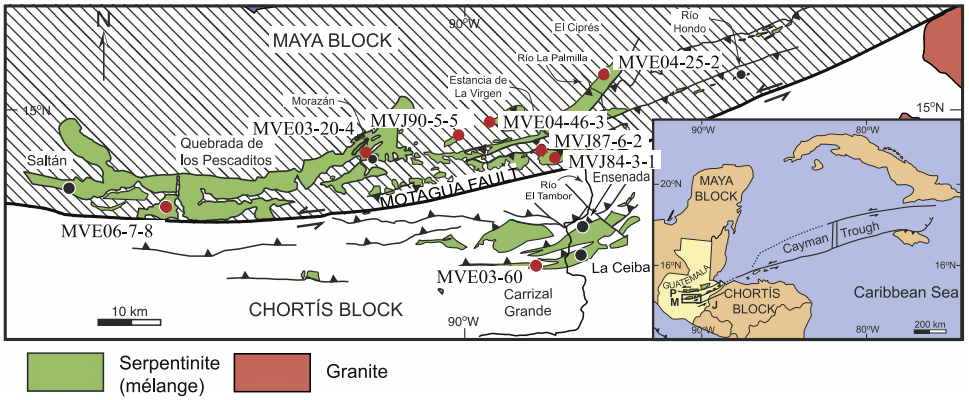

Fig. 1. Locations (red dots) of the studied antigorite samples from the Motagua fault zone of central Guatemala. (For interpretation of the references to color in this figure legend, the reader is referred to the web version of this article.)

Table 1
Sample locations and descriptions.

Sample ID	Lat/Lon	Description
MVE03-60	14.848 N/89.940 W	Fine-grained antigorite serpentinite with minor (< 1–3%) magnesite, talc, chromite, and Ni-sulfides. Dolomite (in vein; < 1% of total) identified by EDS and EBSD. Talc intergrown with antigorite caused polishing problems. Mixed brittle deformation with shear crystallization of atg; weak foliation, no lineation.
MVE04-25-2	15.012 N/89.816 W	Mixed medium- (~100μm × 5 μm) and fine-grained (< 50μm × 1 μm) antigorite serpentinite with minor Mg-chlorite, talc, chromite, Mn-ilmenite, Fe–Ni-sulfides, and dolomite. Mare's tail and cross vein Atg. Little deformation, late brittle fracturing; weak foliation, no lineation.
MVJ90-5-5	14.946 N/90.007 W	Fine-grained (~100μm × 2–5 μm needles) antigorite serpentinite with minor brucite, magnesite, Mn-ilmenite, pentlandite, and dolomite. Splaying bundles of antigorite, magnesite, and dolomite. Little deformation; weak foliation, no lineation.
MVE04-46-3	14.991 N/89.958 W	Fine-grained (~100μm × 2–5 μm) antigorite serpentinite with minor Mn-ilmenite. Mesh texture Atg. Recrystallized (?); weak foliation, no lineation.
MVJ87-6-2	14.941 N/89.885 W	Medium-grained (~200μm × 20 μm) antigorite serpentinite with minor magnetite, Mn-ilmenite, and dolomite. Mesh texture Atg. Recrystallized (?); weak foliation, no lineation.
MVE06-7-8	14.853 N/90.343 W	Medium (~150μm × 50 μm) to fine-grained (< 10 μm) antigorite serpentinite with minor magnesite, magnetite, pentlandite, pyrrhotite, and Ni metal. Brittle deformation (?) w/recrystallized Atg (?); weak foliation, no lineation.
MVJ84-3-1	14.942 N/89.852 W	Medium (~200μm × 50 μm) to fine-grained (~100μm × 5 μm) antigorite schist with minor magnesite and chromite. Identifiable foliation, weak lineation defined by preferred orientation of antigorite grains in thin section.
MVE03-20-4	14.940 N/90.164 W	Medium-fine-grained (100μm × 50 μm) antigorite serpentinite with minor magnesite, talc, chromite, Mn-ilmenite, pyrite, and dolomite. Recrystallized mylonite; strong foliation, weak lineation defined by elongated antigorite needles in thin section.

sections were prepared for each sample. We attempted to cut each thin section parallel to the foliation and lineation, but the foliation was difficult to discern in most samples due to fine grain size. The thin sections were polished to 0.25 μm smoothness using diamond polish, and further polished to ~10 nm smoothness using colloidal silica for ~1–2 h. Because antigorite is very soft, all polishing was done incrementally by hand, on a sample-by-sample basis.

2.2. Electron backscatter diffraction (EBSD)

EBSD measurements were made at UCSB in an FEI Quanta 400f scanning electron microscope with a field-emission gun and an Oxford Instruments EBSD camera, using HKL Channel 5 software. The samples were not coated with carbon. EBSD patterns were collected in low vacuum (50–70 Pa), using an accelerating voltage of 20 kV, a spot size of ~1 μm, working distances of 10–15 mm, and with the sample tilted 20° to the incident beam. EDS data were collected simultaneously during EBSD mapping, and were used to ensure proper indexing of patterns. A match unit for EBSD indexing of antigorite was created from the structural data in Capitani and Mellini (2004). A maximum of 7 bands were detected and between 50 and 70 reflectors were used for indexing. The Channel 5 software uses a Hough transform for automated band detection (e.g., Krieger Lassen, 1998; Day, 2008), and Hough space resolution was set between 95 and 110. Three background frames were measured, and 2-by-2 binning was used in the images.

Two types of EBSD maps were made for each thin section. A fine-scale (1–2 μm step size) map was made to image the microstructure at high resolution. The fine-scale maps also allowed assessment of the quality of the polishing and EBSD indexing rates. The fine-scale band-contrast map gave a good measure of the quality of the EBSD patterns being recorded, and provided an excellent image of the microstructure even when indexing rates were low. No post-processing 'cleaning' has been applied to any of the fine-scale EBSD maps, and indexing rates reported are for raw data. In addition to the fine-scale EBSD map, a coarse map (~100 μm step size) was measured for the purpose of getting 1-point-per-grain measurements across as much of the thin section as possible for determination of crystal preferred orientation (CPO). A coarse map was not measured for MVE03-60 because little of the sample produced detectable EBSD patterns.

2.3. Seismic-velocity calculations

Seismic velocities were calculated using the method described in Mainprice (1990) as implemented in the FORTRAN software written by David Mainprice. All velocity calculations were done using the CPOs determined from the coarse EBSD maps because